

## TRANSIENT CONTROL OF THE SEPARATING FLOW OVER AN AIRFOIL

George Tak Kwong Woo

George W. Woodruff School of Mechanical Engineering,  
Georgia Institute of Technology  
771 Ferst Drive, Atlanta, GA 30332, USA  
gtkwoo@gatech.edu

Ari Glezer

George W. Woodruff School of Mechanical Engineering,  
Georgia Institute of Technology  
771 Ferst Drive, Atlanta, GA 30332, USA  
ari.glezer@me.gatech.edu

## ABSTRACT

The effects of pulsed actuation on stalled NACA 4415 airfoil is investigated in wind tunnel experiments. The actuation results in transitory flow attachment that is manifested by rapid changes in the global circulation and aerodynamic forces. Actuation is applied by a momentary [O(1 msec)] jet produced by a combustion-based actuator such that the characteristic duration of the impulse is an order of magnitude shorter than the characteristic convective time over the airfoil. The present work has shown that large-scale changes in vorticity accumulation and flux can be effected by successive repetitions of a single actuation pulse and are accompanied by significant shedding of CCW vorticity concentrations on the pressure side coincidentally with the trapping of CW vorticity concentrations, hence extending the streamwise domain of the attached vorticity layer towards the trailing edge.

## BACKGROUND

Traditional approaches to control of separation on stalled airfoil have focused on quasi-steady actuation within two distinct frequency regimes. “Low-frequency” actuation has relied on receptivity of the separated, wake-dominated flow to external actuation within a narrow-band of Strouhal numbers that effectively correspond to unstable frequencies of the near wake,  $St_{act} \sim O(1)$  (e.g., Neuburger and Wynanski, 1987, and Seifert et al., 1996).

“High-frequency” actuation is decoupled from global flow (wake) instabilities and emphasizes fluidic modification of the “apparent” aerodynamic shape of the surface upstream of separation at actuation frequencies that are at least an order of magnitude higher than the characteristic wake frequency [i.e.,  $St_{act} \sim O(10)$ ] (e.g., Honohan et al., 2000, and Glezer et al., 2005). Actuation is effected by forming a controlled interaction domain of trapped vorticity between a surface-mounted fluidic actuator and the cross flow above the surface that displaces the local streamlines of the cross flow and thereby induces a ‘virtual’ change in the shape of the surface.

The separated flow is extremely susceptible to transitory actuation such that substantial control authority can be achieved when the actuation input is applied on time scales

that are significantly shorter than the characteristic advection time over the separated flow domain. Brzozowski and Glezer (2006) exploited the receptivity of separated flow over a stalled airfoil and showed that a single actuation pulse [O( $0.05T_{conv}$ )] could lead to brief, partial collapse of the separated flow domain and a momentary increase in circulation on time scale of  $10T_{conv}$ . The recent work of Woo et al. (2008) demonstrated significant pressure and lift recovery of a stalled airfoil with successively pulsed actuation that are applied  $T_{conv}$  apart, and with burst-modulated actuation. The present work is motivated by the previous investigations of pulsed actuation. The major focus of the present work is on the transient aerodynamic effects of repetitive pulsed actuation on the separated flow over an airfoil. Current work also explores the dynamics of the actuation on the large coherent structures in the separating shear layer, and their role in the momentary attachment.

## EXPERIMENTAL SETUP AND PROCEDURES

The experimental setup is described in detail in the earlier work of Woo et al. (2008). The 2-D airfoil (Figure 1a) has a fixed cross section based on a NACA 4415 configuration ( $c = 457$  mm, 1 m span). The airfoil model is comprised of three spanwise segments where the center segment is instrumented with a spanwise array of seven combustion-based jet actuators. The center section is also instrumented with 75 static pressure ports located circumferentially at mid-span.

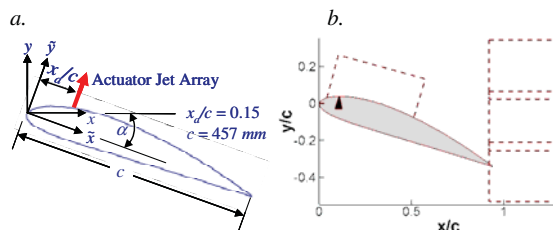


Figure 1. a) Coordinate systems for airfoil model with integrated combustion actuators located at  $x_d/c = 0.15$ . b) Map of PIV frames used for experiments. Location of actuators is indicated by the solid triangle.

All experiments are conducted in an open return wind tunnel at the Fluid Mechanics Research Laboratory at the Georgia Institute of Technology. The tunnel test section measures 1 x 1 m and it is set to a free stream velocity,  $U_0 = 20$  m/s ( $Re_c = 570,000$  based on the chord length). The convective time scale of the flow, at this velocity, over the airfoil is  $T_{conv} = 25$  msec and the airfoil begins to stall at angles of attack exceeding  $17^\circ$  in the absence of actuation. In the present experiments, the airfoil is set at an angle of attack of  $\alpha = 20^\circ$ . At this angle, the flow separates at  $x/c \approx 0.2$  in the absence of actuation. The corresponding lift and drag coefficients are 1.16 and 0.16, respectively.

The actuators each consists of a nominally  $1 \text{ cm}^3$  chamber that combusts a non-premixed mixture of air and hydrogen. Miniature spark generators are used to ignite the mixed reactants in the chambers to produce high-pressure pulsed jets at the orifices. The jet orifices (each measures  $19 \times 0.3$  mm and equally-spaced 3.2 mm apart) are flush-mounted on the suction side at  $x_a/c = 0.15$ . In Woo et al. (2008), the characteristic pressure-time history within the  $1 \text{ cm}^3$  combustion chambers in the actuator array is detailed. The sharp rise in chamber pressure [ $O(1 \text{ ms})$ ], results in a high-pressure jet emanating from the chamber orifice. The chamber pressure peaks and then decreases to atmospheric pressure within 2 – 3 ms following ignition. The short duration of these jets, and their high exit velocities are being exploited here for flow control applications to enhance aerodynamic performances of the stalled airfoil. The development and characterization of these actuators in general is described in detail by Crittenden et al. (2006). The actuators, for the work detailed hereon, are computer-controlled for continuous actuation or for burst-modulated actuation, both characterized by the repetition time between pulses,  $T_{pulse}$ . For burst-modulated actuation, the number of pulses,  $N$ , can be varied.

The flow over the airfoil is characterized using phase-locked, high-speed particle image velocimetry (PIV) in the cross-stream plane  $z = 0$  where the flow is seeded with micron-size smoke particles. For each view, sets of PIV images are captured at a sequence of predetermined time delays relative to the actuation signal. Velocity data within the domain ( $0.05 < x/c < 0.55$  and  $0 < y/c < 0.17$ ) encompassing the actuators and the separation point above the airfoil are collected at  $217.7 \mu\text{m}/\text{pixel}$  (Figure 1b). In the wake, three overlapping windows are used for the PIV measurements at  $212.5 \mu\text{m}/\text{pixel}$  to assess the time-dependent circulation about the airfoil.

## RESULTS

As discussed above, the present work explores the effects of repetitive pulsed actuation on the stalled flow over an airfoil. The global effects are measured by the transitory changes in circulation as an indication of the aerodynamic performance of the airfoil. The dynamics of the actuation are characterized by the manipulation of the large-scale vortical structures following actuation.

### Global Circulation Buildup

In the present experiments a burst of repetitive pulses having a duration of  $20 - 25T_{conv}$  is used to effect flow

attachment using two repetition rates of  $St = T_{conv}/T_{pulse} = 1$  and 2.5. Each burst is followed by an idle period of  $20T_{conv}$  to ensure sufficient time for the relaxation and separation of the attached flow.

The time rate of change of the airfoil's circulation is computed by integrating the vorticity flux across the wake  $d\Gamma/dt = \int u \cdot \omega dy$ , and the global change in circulation relative to the baseline (unforced) flow,  $-\Delta\Gamma(t)/\Gamma_0$ , is computed by integrating  $d\Gamma/dt$  ( $\Gamma_0$  is the baseline circulation). Figure 2 shows the normalized circulation  $-\Delta\Gamma(t)/\Gamma_0$  for the two actuation schemes. The corresponding actuation signals are superimposed for reference.

In both cases shown in Figure 2, for each pulsed jet ejected by the actuators into the boundary layer of the airfoil, a CW vortex is shed from the airfoil's top surface and is advected past the measuring station in the wake. This CW vorticity flux results in a local peak in  $|\text{d}\Gamma/\text{d}t|$  from the top surface as discussed in Woo et al. (2008). The CW negative vorticity flux from the top surface decreases as the wake narrows after the passage of each CW vortex as indicated by subsequent oscillation peaks. These oscillations continue until the flow begins to accumulate negative vorticity as it slowly relaxes to its stalled state due to the absence of actuation.

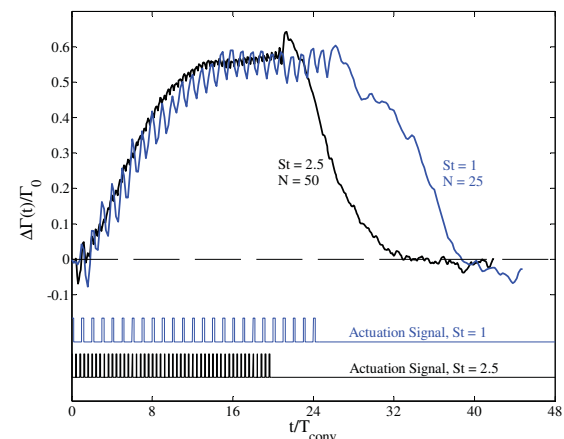


Figure 2. Time-dependent incremental change in circulation following 25 pulses at  $St = 1$  and 50 pulses at  $St = 2.5$ . Actuation signals are shown.

Shedding of CCW vortices from the pressure side occurs for each actuation pulse. The positive vorticity associated with each CCW vortex results in a local peak in  $|\text{d}\Gamma/\text{d}t|$ , followed by the accumulation of positive vorticity as the flow relaxes to the stalled state. The circulation traces in Figure 2 consist of an initial period of rapid circulation buildup followed by a period of saturation at a level of approximately 55% above the stalled flow. Although the rate of increase in circulation for the initial evolution phase is somewhat faster for  $St = 2.5$  than for  $St = 1$ , the duration of actuation needed to reach this maximum circulation level is similar for both repetition rates ( $t/T_{conv} \sim 15$ ), hence it takes about 35 pulses at  $St = 2.5$  compared to 15 pulses at  $St = 1$ . However, the slow relaxation process for both traces are similar, requiring about  $15 T_{conv}$  for the flow to return to the stalled state.

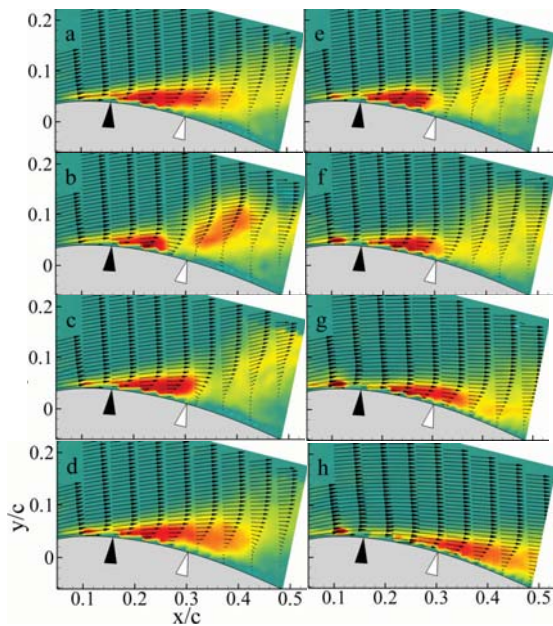


Figure 3. Phase-averaged raster plots of normalized spanwise vorticity and velocity vectors for  $St = 1$ . Actuator location marked by solid triangles, baseline boundary layer separation by open triangles. Times after actuation trigger are  $t/T_{conv} = 0$  (a), 0.44 (b), 0.6 (c), 0.88 (d), 1.52 (e), 2.52 (f), 12.52 (g), and 24.96 (h). Normalized vorticity contour levels: -40 to 40

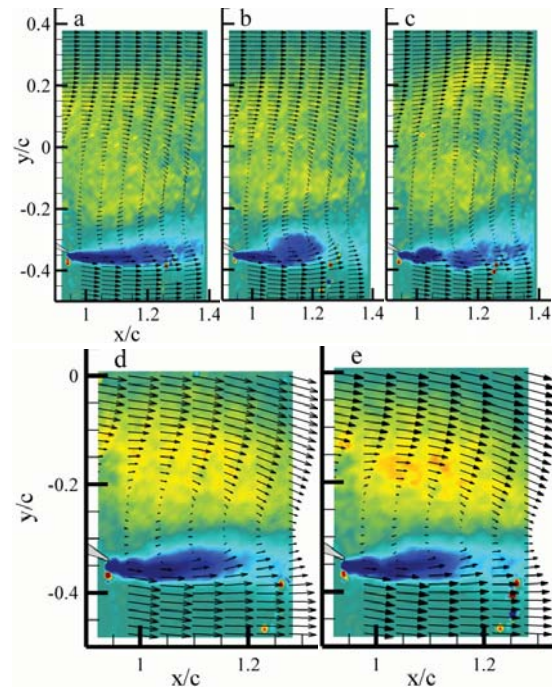


Figure 4. Phase-averaged raster plots of normalized spanwise vorticity and velocity vectors in the wake for  $St = 1$ . Times after actuation trigger are  $t/T_{conv} = 0$  (a), 0.8 (b), 1.4 (c), 13.2 (d), and 25.2 (e). Normalized vorticity contour levels are the same as in Figure 3.

The strong alternating CW and CCW vortices are associated with reduction and increase in global circulation as measured in the wake. The time-periodic repetition results in a flow that is similar to a time-harmonically-forced flow. As shown in Figure 2, these oscillations are approximately 75% smaller for  $St = 2.5$  than for  $St = 1$ . The reduced oscillation magnitudes and the larger number of pulses needed to reach the pseudo-saturated level with increasing  $St$  is due to the interactions of the vortical structures that are effected by the actuation pulses as they are advected downstream on the suction side of the airfoil. These interactions and the details of the mechanism that manipulates the separated layer are discussed in the next section.

The normalized spanwise vorticity concentrations in the vicinity of the actuators on the suction side of the airfoil, and in the wake are shown in Figures 3 and 4, respectively. The separated baseline flow field in this measurement domain and in the wake is shown in Figures 3a and 4a for  $t/T_{conv} = 0$ , respectively. The actuators (solid triangle) is positioned upstream of separation (open triangle). The starting CCW vortex following the onset of actuation is shown in Figure 4b. An example of the CW vortices that are shed by each actuation pulse is clearly visible in Figure 3b, which shows the CW vortex shed by the first pulse for  $St = 1$  at  $t/T_{conv} = 0.44$ . This vortex is advected towards the trailing edge as shown in Figure 3c at  $t/T_{conv} = 0.6$  after actuation. By  $t/T_{conv} = 0.88$  (Figure 3d) after actuation, this vortex is no longer visible within the measurement domain,

and it is first detected in the wake at  $t/T_{conv} = 1.4$  (Figure 4c). The corresponding CW vortices shed by the successive pulses are similar and are advected downstream (Figures 3e-g). The boundary layer within the measurement domain is now attached after the 25<sup>th</sup> pulse at  $t/T_{conv} = 24.96$  (Figure 3h). The details of the formation and advection of the CW vortices and other induced structures in the shear layer are discussed in the next section. In the wake, the vorticity concentrations and velocity vectors show significant vectoring of the flow above the airfoil towards its suction surface after the 13<sup>th</sup> and 25<sup>th</sup> pulses (Figures 4d and e, respectively). This suggests that the wake is narrower as a result of the pulse repetition of single pulses. It becomes almost time-invariant after the 15th pulse as suggested by the circulation time trace in Figure 2.

Figure 5 shows phase-averaged cross stream wake distributions of the normalized streamwise and cross stream velocity components, the spanwise vorticity, the turbulent kinetic energy, and the vorticity flux for  $St = 1$  at  $x/c = 1.1$  (i.e. 0.15c from the trailing edge of the airfoil). The baseline flow at  $t/T_{conv} = 0$  is shown in Figure 5a. Shortly after actuation at  $t/T_{conv} = 1.4$ , the cross stream velocity distribution changes dramatically as the first CW vortex is advected into the measurement domain (Figure 5b). This instant in time corresponds to that shown in Figure 4c.

By  $t/T_{conv} = 13.2$  (Figure 5c), there is considerable vectoring of the flow towards the airfoil suction surface and the wake is now narrower, as indicated by the cross stream and streamwise distribution of the velocity components. The

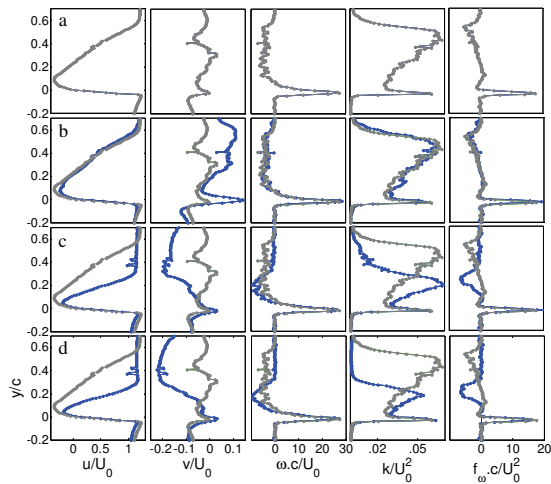


Figure 5. Cross stream wake distributions of the normalized streamwise velocity,  $u/U_0$ , cross-stream velocity,  $v/U_0$ , vorticity,  $\omega_c/U_0$ , turbulent kinetic energy,  $k/U_0^2$ , and the vorticity flux,  $f_{\omega_c}/U_0^2$  in the near wake at  $x/c = 1.1$  from the leading edge of the airfoil. Times after actuation trigger are  $t/T_{conv} = 0$  (a), 1.4 (b), 13.2 (c), and 25.2 (d). The baseline case is shown in grey for reference.

high levels of the vorticity, the turbulent kinetic energy and the vorticity flux in the center section of the wake also indicate that the wake is narrower. The wake at this instant in time corresponds to that shown in Figure 4d. The same, but more pronounced global effects are also observed in the wake at  $t/T_{conv} = 25.2$  (Figure 5d) after the 25<sup>th</sup> actuation pulse, which corresponds to the wake shown in Figure 4e.

### Controlled Manipulation of the Separated Flow

The earlier works of Brzozowski et al. (2006) and Woo et al. (2008) suggest that the collapse of the separated domain is accompanied by severing of the separated shear layer and the advection of a large CW vortex. The dynamics of the large vortical structures is further investigated here for the single pulse, and for the three actuation schemes where  $St = T_{conv}/T_{pulse} = 1, 2.5$  and  $3.5$ , all with  $N \leq 10$  pulses. The measurement window above the airfoil shown in Figure 1b is chosen to study the aerodynamic modification of the flow over the airfoil with the focus on the interaction domain between the actuation jet and the cross flow in the vicinity of the actuators.

The characteristics of the flow field above the airfoil can be described in detail within three regions: the interaction domain, the boundary layer and the separated shear layer. The measurement window in the vicinity of the jet orifice is used to provide some details of the boundary layer evolution and the shear layer characteristics.

In order to isolate the structures that are imposed in the flow through the boundary layer, velocity measurements are taken phase-locked to the actuation signal at sequential delays. The normalized vorticity concentrations (Figures 6a-j) show the dynamics within the interaction domain. Note the location of separation (open triangles) relative to the jet orifice (closed triangles). The separated baseline flow

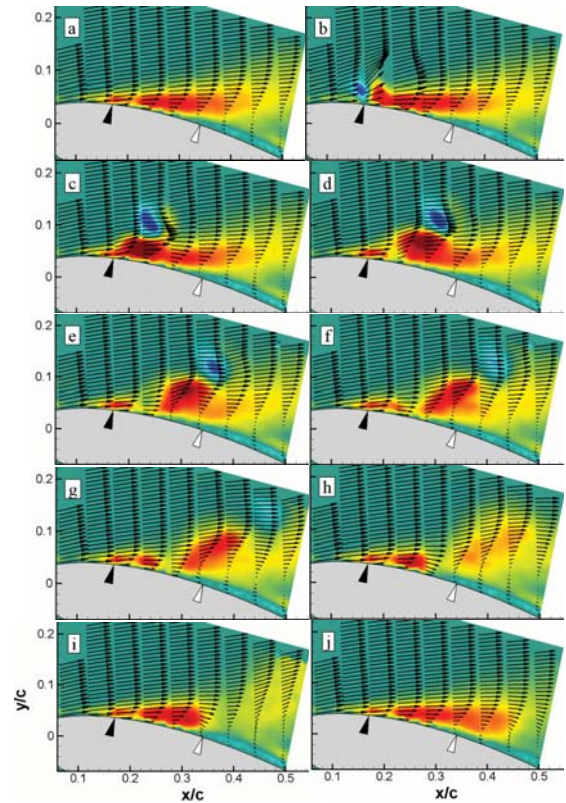


Figure 6. Phase-averaged raster plots of normalized spanwise vorticity and velocity vectors showing the formation of a vortex pair from a single pulsed actuation. Times after actuation trigger are  $t/T_{conv} = 0$  (a), 0.24 (b), 0.28 (c), 0.32 (d), 0.36 (e), 0.4 (f), 0.44 (g), 0.48 (h), 0.6 (i), and 0.74 (j). Normalized vorticity contour levels are the same as in Figure 3.

field in this measurement domain is shown in Figure 6a at  $t/T_{conv} = 0$ . The initial formation of a vortex pair is shown in Figure 6b at  $t/T_{conv} = 0.24$  after the input actuation signal. This inherent delay is between the trigger signal and the combustion process. It is apparent that the momentum of the pulse jet is sufficiently strong so that the vortices can penetrate into the boundary layer, and interact with the separating shear layer.

The ability of these combustion-based jets to alter the aerodynamic characteristics of the lifting surface depends on the local free stream velocity and jet strength. In this early stage of actuation the jet vortex with the clockwise (CW) vorticity is dominant in the presence of the cross flow as explained by Vukasinovic et al. (2005). The strength of this vortex is crucial for the collapse of the shear layer. The imposed CW vorticity merges into the boundary layer. It then coalesces with the separated shear layer to create large scale motions (Figures 6b – d). The abrupt actuation creates a discontinuity in the vorticity field of the shear layer and a new CW vortex is induced. This discontinuity is located at  $x/c = 0.2$  in Figure 6d and becomes more visible at  $x/c = 0.25$  by  $t/T_{conv} = 0.44$  (Figure 6g). By disrupting the boundary layer, the small scale CW vortex induces a large

CW vortex through a rollup process (Figures 6c – e). While the large structure grows along the wall of the airfoil, the small CCW vortex, which is formed by the pulse is advected downstream above the shear layer. By  $t/T_{conv} = 0.48$  (Figure 6g) following actuation, the CCW vortex has moved out of the measurement domain.

As the induced CW structure dissipates, it continues to move downstream from the actuators (Figures 6g–i). The induced large scale motions associated with the formation of this CW structure create a two-domain flow regime above the airfoil. The separating layer is now completely severed from the upstream attached boundary layer (Figure 6e). The front of this *new* boundary layer begins to move towards the trailing edge (Figures 6f – j), creating a larger region of attached flow above the airfoil (compare Figures 6j and a). Following the end of the actuation (Figure 4j), the boundary layer recovers and the shear layer slowly returns to the separated unforced state as detailed by Woo et al. (2008).

Figure 7 shows the corresponding  $x-t$  evolution of vorticity flux for the same domain above the airfoil. It emphasises the formation and the subsequent dissipation of large-scale motions that are induced by the direct small-scale motions in the flow upon the onset of the actuation.

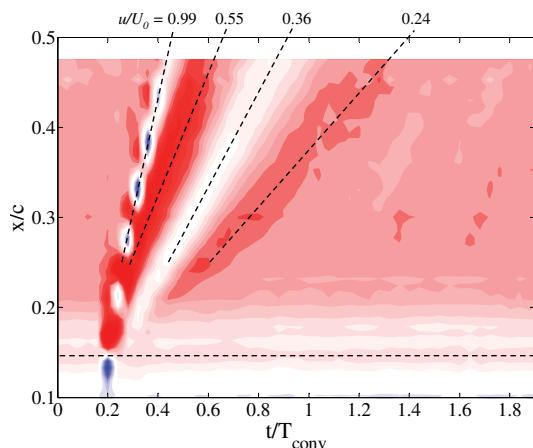


Figure 7. Vorticity flux plot for single pulsed actuation showing propagation velocities of the direct vortex pairs and the induced coherence CW structure. Normalized vorticity flux contour levels: -1.5 to 0.5

The measurements indicate that the small-scale CW vortex and the large-scale structure are advected downstream at  $u/U_0 \approx 0.99$  and  $0.55$ , respectively. The severed region between the attached upstream boundary layer and the downstream recirculating region is growing in size, and its front is moving at a slower speed of  $u/U_0 \approx 0.36$ , which corresponds to the propagation velocity of the “peak” adverse pressure gradient.

### Successive Pulsed Actuation

The present work is motivated by the differences in the transitory response of the flow to different repetition rates of the actuation pulse as evident in circulation time traces for

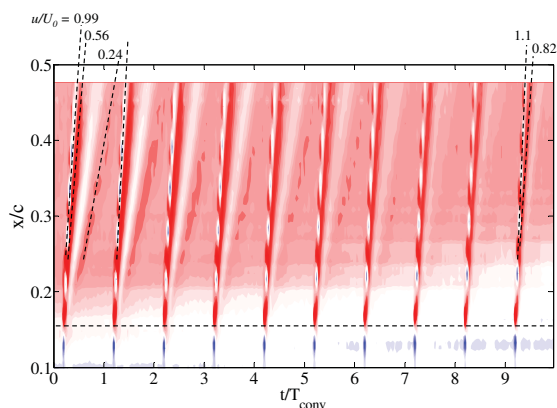


Figure 8. Vorticity flux plot for 10 successive pulsed actuation with  $St = 1.0$  showing differences in propagation velocities of structures. Normalized vorticity flux contour levels are the same as in Figure 7.

$St = 1$  and  $2.5$  (Figure 2), and by the differences in the circulation buildup between a single pulse and repeated pulses reported by Woo et al. (2008).

In this section, the transitory manipulation of the separated shear layer is first investigated for the case  $St = 1$ . As consistent with the data of Woo et al. (2008) it is shown that separation is increasingly delayed by each successive pulse. The boundary layer becomes thinner and the separation point moves farther downstream with more actuation at  $St = 1$ . It is also noted that the onset of the severing of the separated vorticity layer by the CW actuation vortex migrates farther downstream from the orifice with each pulse. This is due to the fact that the streamwise pressure gradient is modified by the previous actuation in such a way that the “peak” adverse pressure gradient moves downstream with each pulse, hence the forced flow can withstand higher adverse pressure gradients than the baseline flow.

As in the case for  $St = 1$ , the above features are observed for  $St = 2.5$  and  $3.5$ . Although the flows are similar for these cases there are significant differences in the dynamics of the control mechanism. It is apparent from the  $x-t$  vorticity flux plots (Figures 8 and 9) that for  $St \geq 1$ , there are interactions between the actuation CW vortices and the large-scale coherent CW vortex. This is due to the rapid repetition of the next pulse. For  $St = 1$  (Figure 8), these interactions are not evident in the measurement domain, but the differences in propagation velocities of the structures leads to the interaction between the direct CW vortices and the coherent structures downstream of the measurement domain. Due to the shorter delay between the pulses for  $St = 2.5$  and  $3.5$ , the interaction domains are now within the measurement domain (Figure 9). The interaction region is closer upstream to the jet orifice for each pulse for  $St = 3.5$  than it is for  $St = 2.5$ .

From these observations, it is apparent that the increased suppression of the large coherent structures with the faster moving CW actuation vortices at higher repetition rates (increasing  $St$ ) explains the smaller oscillations for  $St = 2.5$  than for  $St = 1$  in the circulation trace in Figure 2. The interactions also explain the higher initial circulation

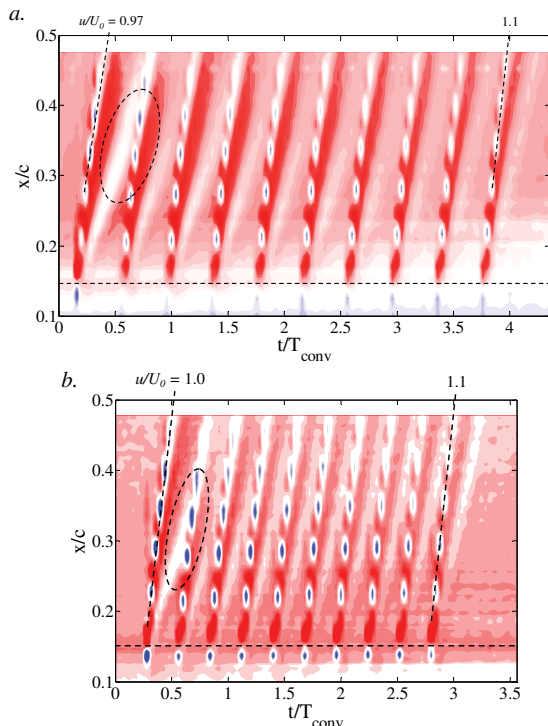


Figure 9. Vorticity flux plot for 10 successive pulsed actuation at  $St = 2.5$  (a) and  $3.5$  (b), showing interaction regions between the structures within the measurement window. Dashed circle indicates the first interaction domain. Normalized vorticity flux contour levels are the same as in Figure 7.

level observed following a single pulse than for the first pulse of actuation burst at  $St = 1, 2.5$  and  $3.5$ . By increasing the jet velocity of the actuation, as discussed above, it is suspected that the actuation CW vortex is ejected further towards the freestream hence its interactions with the separating shear layer and the induced large coherent structures are somewhat delayed, hence reducing the suppression of the large CW vortices on the suction side of the airfoil.

## CONCLUSIONS

The effects of pulsed actuation on stalled flow for a NACA 4415 airfoil is investigated in wind tunnel experiments. It is shown that the actuation results in transitory flow attachment that is manifested by rapid changes in the global circulation and aerodynamic forces. Actuation is applied by a momentary [O(1 msec)] jet produced by a combustion-based actuator such that the characteristic duration of the impulse is on a time scale that is an order of magnitude shorter than the characteristic convective time over the flow. The present work has shown that large-scale changes in vorticity accumulation and flux can be effected by successive actuation pulses and are accompanied by significant shedding of CCW vorticity concentrations.

The dynamic response of the stalled flow to a single-pulse actuation is rather remarkable. The flow transients

associated with the onset of single-pulse actuation can be exploited to enhance the actuation effectiveness and hence the aerodynamic performance of the airfoil. In particular the relatively long stall relaxation process following the termination of the actuation and the fast dynamic response associated with the reattachment process allow for low duty cycle actuation that is timed to prevent full stall between actuation pulses while sustaining a slow momentary decrease in circulation. These actuation dynamics appear suitable for the implementation of flow control methodology for controlling and mitigating transitory stall such as the time periodic stall on retreating rotorcraft blades.

Repeated actuation of a pulse burst with repetition  $St = 1$  reaches the saturation circulation level by  $t/T_{conv} = 14$  after the onset of the actuation with a 55% increase in lift from the stalled baseline case. The time needed for the  $St = 2.5$  case to reach this plateau level is somewhat shorter, (but corresponds to the 35<sup>th</sup> pulse). In addition to this, the oscillations in the circulation of the airfoil for  $St = 2.5$  is about 25% of that for  $St = 1$ . This is due to the slow down of the growth of the lift-inducing large coherent CW vortex that are formed by the actuation pulses. The growth suppression is a direct result of the interactions between the direct small-scale CW vortices ejected into the separating shear layer by the actuators and the large coherent structures.

The present work has shown that the application of successive actuation pulses can extend the streamwise domain of the attached vorticity layer towards the trailing edge and at the same time lead to a desirable cumulative increase in the transitory circulation. The cumulative increase in circulation depends on the time and location of the interaction regions. It is conjectured that an increase in the jet momentum is beneficial to delaying the interaction, and hence may result in a higher rate of circulation increase.

## REFERENCES

- Brzozowski, D., and Glezer, A., 2006, "Transient Separation Control Using Pulse-Combustion Actuation", *AIAA Paper*, 2002-3166.
- Honohan, A., Amitay, M., and Glezer, A., 2000, "Aerodynamic Control using Synthetic Jets," *AIAA Paper*, 2000-2401.
- Neuberger, D., and Wygnanski I., 1987, "The Use of a Vibrating Ribbon to Delay Separation on Two Dimensional Airfoils", *Proceedings of Air Force Academy Workshop in Unsteady Separated Flow, Report TR-88-0004*, Colorado Springs, CO.
- Seifert, A., Darabi, A., and Wygnanski, I., 1996, "Delay of airfoil stall by periodic excitation", *Journal of Aircraft*, 33(4), pp.691-698.
- Vukasinovic, B., Lucas, D. G., and Glezer, A., 2005, "Controlled Manipulation of Small- and Large- Scales in a Turbulent Shear Layer, Part I: Experimental Studies", *AIAA Paper*, 2005-4753.
- Woo, G., Crittenden, T., and Glezer, A., 2008, "Transitory Control of a Pitching Airfoil using Pulse Combustion Actuation", *AIAA-Paper, AIAA 4th Flow Control Conference*, Seattle, WA, 2008-4324.